Variation of electronic and atomic structures in $YBa_2(Cu_{1-x}Fe_x)_3O_{7-\delta}$

C. Y. Yang,* S. M. Heald, J. M. Tranquada, Youwen Xu, Y. L. Wang, A. R. Moodenbaugh, D. O. Welch, and M. Suenaga

Department of Applied Science, Brookhaven National Laboratory, Upton, New York 11973

(Received 16 November 1988)

We present x-ray-absorption spectroscopy measurements of $YBa_2(Cu_{1-x}Fe_x)_3O_{7-\delta}$, $x=0.015$ to 0.15. Both near-edge features and extended x-ray-absorption fine-structure (EXAFS) results demonstrate that Fe preferentially substitutes for Cu(1) atoms at the linear-chain site. The compositional trend of these samples shows that the valence state of Fe (mainly +3, but the possible presence of small amounts of +2 and +4 cannot be ruled out) remains the same and Fe—O bond lengths change minimally in the light of changes in the lattice parameters with composition. Because of its sensitivity to coordination geometry, the reduction of the intensity of the $1s \rightarrow 3d$ edge feature indicates that the average coordination number of Fe nearest neighbors increases with increasing Fe content. EXAFS data analysis also finds an increase in the number of oxygen neighbors in the linear-chain plane, indicating an introduction of the extra oxygen atom on the vacancies of the a axis. Based on statistical considerations, we have examined the distribution of this extra oxygen atom as well as three possible Fe site coordination geometries (fourfold, fivefold, and sixfold).

I. INTRODUCTION

The investigation of Fe substitution in the high-T_c superconductor system $YBa_2(Cu_{1-x}Fe_x)_3O_{7-\delta}$ is of considerable interest, and the changes induced by Fe have been extensively reported.[1-10] Substitution of Fe leads to a lowering of T_c, a structural phase transformation, an increase in oxygen content accompanied by a rearrangement of oxygen, and a local magnetic ordering. However, how these changes are correlated is still not well understood. For example, it is known[1-2] that a small change in Fe content from $x=0.02$ to $x=0.03$ can give rise to a structural change from orthorhombic to tetragonal symmetry. But this change has a relatively small influence on the behavior of T_c in the vicinity of the orthorhombic-tetragonal transition, indicating a remarkable insensitivity of T_c to crystal symmetry. As the Fe concentration is increased beyond $x=0.05$, T_c starts to decrease rapidly, but superconductivity persists at low temperature even with a significant amount of Fe ($x=0.10$–0.15). By nature, Fe is most likely to go into the Cu sites rather than Y or Ba sites because of the similarity of the electronic configurations and atomic size. In fact, several neutron and x-ray scattering measurements[2-6] as well as Mössbauer studies[2,7-9] confirm this point. When Cu is replaced by Fe, the oxygen atoms might rearrange themselves in order to provide the most stable Fe site with a specific local configuration. Furthermore, the modification of the local electronic densities of states and the valences is also anticipated. Unfortunately, detailed information concerning all these factors, which may be closely related to superconductivity, is limited.

The orthorhombic $YBa_2Cu_3O_7$ has two distinct Cu sites, the linear-chain site and the planar site, labeled as Cu(1) and Cu(2), respectively. It is important to determine whether Fe substitutes into one or both Cu sites. There have been, however, various interpretations regarding the identity of the Fe site, as well as the determination of the valence state, among Mössbauer investigators.[2,7-9] On the other hand, neutron and x-ray diffraction results[2-6] generally agree that Fe resides only or predominately on the Cu(1) site. There is little agreement on the value of Fe—O bond lengths. In this work we use x-ray absorption spectroscopy (XAS) techniques to clarify these issues.

With the XAS technique, one can determine the average environment of the dilute Fe atoms by tuning the x rays to the Fe K-edge absorption energy; samples with very low Fe concentration, which pose difficulties for traditional techniques, can easily be studied using fluorescence detection. The x-ray absorption spectrum can be divided into two distinct regions: (1) the near-edge structure, within about 30 eV of threshold, which contains information about the valence of the absorbing atom, ligand types, and site geometry, and (2) the extended x-ray absorption fine structure (EXAFS), which may extend more than 1000 eV above the edge and which provides direct structural information. Thus, the goal of this XAS work is to quantify the influence of the Fe substitution on the electronic and atomic structures in $YBa_2(Cu_{1-x}Fe_x)_3O_{7-\delta}$.

This paper reports an XAS study of the Fe site in $YBa_2(Cu_{1-x}Fe_x)_3O_{7-\delta}$. Section II deals with sample preparation, characterization, and experimental details of the XAS measurements. Section III presents the results and discussion of the electronic and atomic structural changes induced by the substitution of Fe. Interpretation of XAS results allows us to develop several statistical models to examine the distribution of oxygen atoms as well as to test three possible Fe site geometries at all concentrations. A brief summary (Sec. IV) concludes this paper.

II. EXPERIMENT

A. Sample preparation and characterization

$YBa_2(Cu_{1-x}Fe_x)_3O_{7-\delta}$ ($x=0.015$, 0.02, 0.03, 0.05, 0.10, and 0.15) specimens were prepared by mixing the appropriate amounts of Y_2O_3, $BaCO_3$, CuO, and Fe_2O_3 powders. The powders were ground thoroughly, pressed into pellets, and fired in air at 900 °C twice. They were then heated in flowing oxygen at 970 °C for more than 40 h, annealed at 650 °C for 8 h, and then furnace cooled to below 100 °C.

The superconducting transition temperature T_c was measured by mutual inductance. X-ray-powder diffraction scans were obtained with a conventional setup using Cu $K\alpha$ radiation and diffracted beam monochromator. All the samples with Fe content $x=0.015$ to 0.15 showed no observable impurity peak above the 2% level of detection in the x-ray-diffraction diagram. T_c and lattice parameters as a function of Fe content are listed in Table I. T_c as well as the lattice parameters varies with Fe concentration. For $x \leq 0.03$, T_c changes little, while above $x > 0.05$, T_c smoothly falls as Fe content increases. Samples with $x < 0.03$ are found to have an orthorhombic structure. When the structural phase transition from orthorhombic to tetragonal occurs at ($x \geq 0.03$), c slightly decreases. This implies that variation[4-6] of oxygen content may occur at higher Fe concentrations. The chemical composition of the sample was checked by electron microprobe analysis using a wavelength dispersive spectrometer. Transmission electron microscopy (TEM) was also used to elucidate microstructural changes of these specimens. A preliminary TEM result was reported earlier;[10] the details of TEM data will be presented elsewhere.[6]

The unoriented XAS samples were ground to fine powders to pass 400 mesh, and then spread uniformly onto Kapton tape. About 6–8 layers of tape were used to make samples with sufficient thickness for the XAS measurements. For performing orientation-dependent x-ray absorption studies, uniaxially oriented specimens ($x=0.05$, 0.10, and 0.15) were fabricated in the same manner as described in our previous work.[11] For $x=0.05$, there are small changes in the polarized XAS spectra of about 0.2 eV in the edge position, but other changes of near-edge features are less clear cut. However, no strong orientation dependence of near-edge structure is found for the other two samples ($x=0.10$ and 0.15) at the Fe and Cu K edges. We feel that this could be in part due to the fact[6,10] that the grain size of samples drastically decreased at $x > 0.03$. In this work, the average particle sizes for samples $x=0.10$ and $x=0.15$, sieving to 400 mesh, are about four and five times larger than their average grain sizes, respectively. Hence, each particle may contain many misoriented grains, thus making a uniform alignment difficult. The Laue transmission technique confirmed a low degree of orientation (less than 10%) of these specimens. In order to uniquely determine the particle size effect, additional and careful polarized XAS measurements are currently underway.

TABLE I. T_c and lattice parameters of $YBa_2(Cu_{1-x}Fe_x)_3O_{7-\delta}$; T_c is midpoint of ac susceptibility measurement.

x	T_c (K)	a (Å)	b (Å)	c (Å)
0.000	90.5	3.820	3.885	11.676
0.015	87.5	3.829	3.881	11.678
0.020	86.5	3.834	3.897	11.677
0.030	83.0	3.852	3.861	11.686
0.050	75.0	3.861		11.676
0.100	36.0	3.867		11.668
0.150	<4.2	3.873		11.660
Uncertainty	± 0.5	± 0.002	± 0.002	± 0.002

B. X-ray absorption measurements

The x-ray absorption spectra of the Fe K edge were collected at the X-11A beam line at the National Synchrotron Light Source (NSLS). During this run NSLS was operated at an energy of 2.5 GeV and electron current from 40 to 100 mA. Energy selection was accomplished by using a double-crystal monochromator with Si(111) crystals. The photon energy was initially calibrated from the first inflection point of an Fe foil. In this experiment, FeO was placed after the samples to provide simultaneous calibration. The monochromator was detuned by reducing the incident photon flux about 20% in order to suppress contamination from harmonics. Using an incident beam slit to limit the size of the beam (excluding scattered radiation and improving energy resolution), the beam size was approximately 1×8 mm^2. At the X-11A beam line, an energy resolution appeared to be on the order of ~ 3 eV at the Fe K edge. The data were measured in fluorescence mode with a nitrogen-filled ion chamber to monitor incident photon flux and an argon-filled fluorescence detector[12] to monitor the Fe $K\alpha$ x rays. The standard iron compounds, FeO, Fe_3O_4, α-Fe_2O_3 (hematite), ferrous oxalate dihydrate (Fe^{2+} oxalate), $FeC_2O_4\cdot 2H_2O$, ferric oxalate (Fe^{3+} oxalate), and $Fe(H_2O)_6$ [$Fe(NO_3)_3$ in $0.1n$ HNO_3], were measured in earlier runs.[13] The high-valent Fe^{4+} data[14] of horseradish peroxidase, (HRP), designated as Fe-HRP was provided by Dr. J. Penner-Hahn. Energy of these spectra was calibrated to the first inflection point of an Fe foil. The iron glycine [tin-μ3-triaquo-hexakis(glycine)-tri iron (III) perchlorate] data,[15] designated as Fe-glycine, was provided by Dr. G. Bunker. All spectra were taken at room temperature.

III. RESULTS AND DISCUSSION

The physical mechanism of the x-ray absorption process as a function of energy can be understood from the Fermi "golden rule." In this approximation,[12] the absorption coefficient can be represented by

$$\mu(E) \propto |M|^2 \rho(E) . \quad (1)$$

$|M|$ is a dipole matrix element and $\rho(E)$ is the projected density of states above the Fermi level corresponding to the photoelectron energy E. At energies near the absorption threshold, the fine structure is determined predom-

inantly by the local density of states. In a poorly screened material, these features are atomiclike in character. Transitions to the continuum tend to give a smooth, broad step in the absorption. At a K edge, the dipole selection rule requires transitions from the initial $1s$ state to have p symmetry. When a narrow, unoccupied band of d states exists near the Fermi level, as in transition metals, a $1s \rightarrow d$ symmetry feature is observed due to quadrupole transitions. Hybridization between d and p symmetry states can make the $1s \rightarrow d$ feature dipole allowed. The relative energies of the near-edge features are sensitive to the electronic charge (i.e., valence) of the absorbing atom. Molecular-orbital theory[12,16,17] can be useful for interpreting the empirically observed trends of near-edge features versus valence.

Unlike the near-edge structure, the only possible contribution to EXAFS is the matrix element because the density of states should be that of a free electron which gives only monotonic contributions. The EXAFS oscillations result from interference between the outgoing photoelectron wave function from the x-ray-absorbing atom and the backscattered wave function from the surrounding atoms. Based on this picture, the specific form of the EXAFS equation[12] from single-scattering theory is given by

$$\chi = \frac{\mu - \mu_0}{\mu_0} = -\sum_i A_i(k) \sin[2kR_i + \phi_i(k)] , \qquad (2)$$

where k is the photoelectron wave factor and μ_0 is the smoothly varying atomic background absorption. The sum is over the coordination shells at an average distance R_i and $\phi_i(k)$ is the total phase-shift function due to contributions from both the absorbing and backscattering atoms. The amplitude function $A_i(k)$ is given by

$$A_i(k) = \frac{N}{kR_i^2} F_i(k) e^{-2\sigma_i^2 k^2} e^{-2R_i/\lambda} , \qquad (3)$$

where N_i is the number of scattering atoms in the ith shell, $F_i(k)$ is the magnitude of the backscattering and is a function of the type of scattering atoms, σ_i^2 is the Debye-Waller factor to account for thermal vibrations and structural disorder, and λ_i is the mean free path of the photoelectron. The procedures of data analysis were essentially described in Ref. 12. In the following, we examine the electronic structure and local environment of the Fe site in $YBa_2(Cu_{1-x}Fe_x)_3O_{7-\delta}$.

A. Electronic structure in $YBa_2(Cu_{1-x}Fe_x)_3O_{7-\delta}$

Figure 1 shows representative Fe K-edge absorption spectra of iron oxide model compounds. From left to right they are FeO, Fe_3O_4, Fe_2O_3, and Fe-HRP. These spectra all exhibit two distinct features:[13–21] (1) the small peak below the midpoint of the absorption edge A, which is assigned to the $1s \rightarrow 3d$ transition; and (2) the main peak of the absorption edge B, which corresponds to transitions to unfilled $4p$ states. Two striking trends are apparent in the edge spectra. First, positions of the absorption features shift to higher energy as the valence increases. Second, the intensity of the $3d$ feature varies from compound to compound.

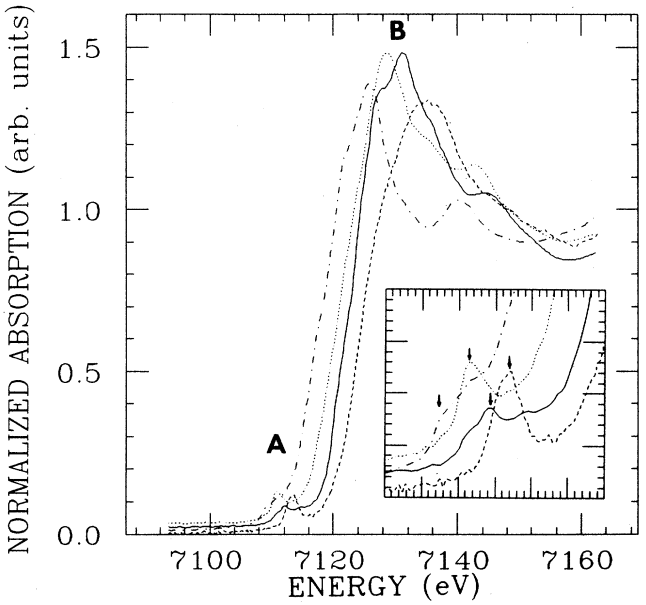

FIG. 1. Fe K-edge absorption for various valence states of iron model compounds: FeO powder (dotted-dashed curve, 2+); Fe_3O_4 powder (dotted curve, mixed 2+ and 3+); α-Fe_2O_3 powder (solid curve, 3+); FE-HRP (Ref. 14) (dashed curve, 4+). The inset gives an expanded view of $1s \rightarrow 3d$ edge features. The peak position of $3d$ features is indicated by the arrow. Simultaneous energy calibration was achieved by using an Fe foil.

The energy shift due to variation in valence state is primarily an electrostatic effect (it will require more energy to remove a core electron as the formal valence increases). The valence states are 2+ for FeO, 3+ for α-Fe_2O_3, and 4+ for Fe-HRP. In going from the ferrous to the ferric oxides, a positive shift in the position of the $3d$ peak (indicated by the arrow) by about 3 eV is exhibited (Fig. 1, Table II). The position of the $3d$ peak for ferro-ferric oxide, Fe_3O_4 (containing Fe^{2+} and Fe^{3+} in the ratio 1:2), lies between the positions of the $3d$ peaks in ferrous oxide (FeO) and ferric oxide (α-Fe_2O_3). A systematic shift of the position of the main peak ($1s \rightarrow 4p$) due to the increase in the valence of iron shows the same trend.

For XAS measurements of $YBa_2(Cu_{1-x}Fe_x)_3O_{7-\delta}$, simultaneous energy calibration was accomplished by using FeO powder. A comparison of the absolute energies of the edge features of Fe in $YBa_2(Cu_{1-x}Fe_x)_3O_{7-\delta}$ with those of FeO indicates that there is a positive shift of 1.8 eV in the $1s \rightarrow 3d$ feature and a positive shift of 2.9 eV in the $1s \rightarrow 4p$ feature from the FeO positions. There is no shift in the $1s \rightarrow 3d$ position with increasing x. The spectra for $YBa_2(Cu_{1-x}Fe_x)_3O_{7-\delta}$ are shown in Fig. 2, with the zero of energy set equal to the position of the $1s \rightarrow 3d$ peaks. The shifts of the $1s \rightarrow 3d$ and $1s \rightarrow 4p$ features relative to FeO suggest that the valence state of substitutional Fe is mainly 3+. However, our current data cannot rule out the presence of small amounts of Fe^{2+} and/or Fe^{4+}. As shown in Fig. 2, the energy positions of A and B remain unchanged with composition. It is important to point out that neither variation of the lattice parameters

TABLE II. Fe K-edge x-ray absorption near-edge structure features for iron oxide model compounds and $YBa_2(Cu_{1-x}Fe_x)_3O_{7-\delta}$.

Compound	Valence state	N	$1s \rightarrow 3d$ intensity[a] (arb. units)	ΔE_A[b] (eV)	ΔE_B[b] (eV)
FeO	2+	6	0.015	0.0	0.0
Fe^{2+} oxalate	2+	6	0.012	−0.5	−2.5
Fe_3O_4	mixed $\frac{1}{3}(2+)$ and $\frac{2}{3}(3+)$	5.3	0.045	1.5	2.5
α-Fe_2O_3	3+	6	0.025	3.0	5.5
$Fe(H_2O)_6$	3+	6	0.023	1.0	3.0
Fe-glycine[15]	3+	6	0.015	. . . [c]	
Fe^{3+} oxalate	3+	6	0.018	1.2	3.7
Fe-HRP[14]	4+	5	0.075	4.2	9.6
$YBa_2(Cu_{1-x}Fe_x)_3O_{7-\delta}$					
$x=0.015$			0.15	1.8	2.9
$x=0.02$			0.15		
$x=0.03$	(Described in		0.14		
$x=0.05$	the text)		0.12	(same)	
$x=0.10$			0.11		
$x=0.15$			0.10		
Uncertainty			±0.01	±0.5	±0.5

[a] The intensity of $3d$ features were determined by subtracting an arc tangent function from the data.
[b] The energy positions of $3d(\Delta E_A)$ and $4p(\Delta E_B)$ features were referred to FeO.
[c] Indeterminate.

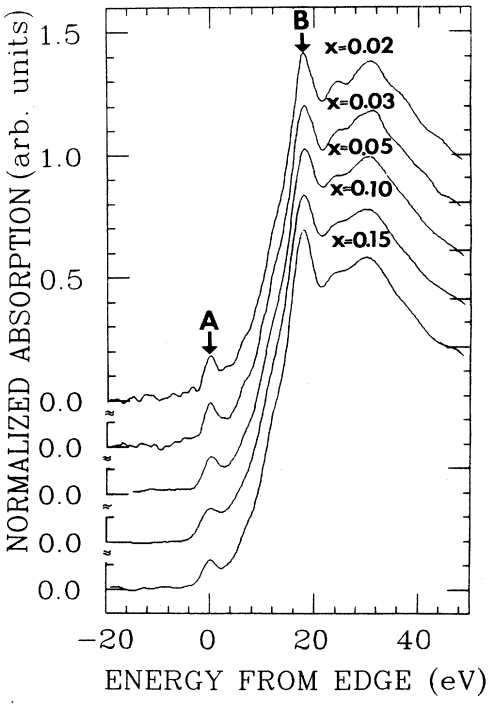

FIG. 2. Fe K-edge absorption spectra for $YBa_2(Cu_{1-x}Fe_x)_3O_{7-\delta}$. The near-edge spectra are shifted in energy to line up the $3d$ peaks. Simultaneous energy calibration was done by using FeO powder. By a comparison the energy position with FeO edge features, the implied valence state of $YBa_2(Cu_{1-x}Fe_x)_3O_{7-\delta}$ is mainly 3+.

with composition nor the phase transformation near $x=0.03$ has any significant influence on the valence of the Fe site.

We now turn our attention to the variation in the intensity of the $1s$ to $3d$ transition. Because both the $1s$ and $3d$ states are centrosymmetric, this transition is forbidden by the dipole selection rule. For the iron site with inversion symmetry, the $3d$ feature is produced primarily by a weaker quadrupole transition. This quadrupole transition has been experimentally demonstrated in the work of polarized Cu K-edge studies.[20] However, if the iron environment is noncentrosymmetric, odd parity states such as p states can hybridize with the d states resulting in a small dipole-allowed contribution at the $3d$ position. The degree of hybridization, and hence, the $3d$ intensity, strongly depends upon the number, nature, and symmetry of the nearest neighbors. Roe *et al.*[21] have recently reported that the intensity of the $1s \rightarrow 3d$ feature of Fe^{3+} compounds varies systematically with coordination number. Using a molecular-orbital (MO) calculation, they showed a good correlation of the $3d$ peak intensity with the total amount of iron $4p$ orbitals mixed into the predominantly iron $3d$ molecular orbitals. The total percentage of the iron $4p$ atomic orbitals mixing with the $3d$ orbital character is found to be 0.4%–4% for 6-coordinate, 11%–13% for 5-coordinate, and 20%–22% for 4-coordinate Fe^{3+}. Thus, integration of the $3d$ peaks gives approximate peak areas for 6 coordinate, 5 coordinate, and 4 coordinate in the ratio 1:2:4.

The variation in the $1s \rightarrow 3d$ intensity due to the effects of site geometry and coordination number is illustrated by the spectra in Fig. 1. The near-edge spectrum of FeO

(NaCl structure) shows a very small $1s \rightarrow 3d$ feature because it has nearly perfect FeO_6 octahedral symmetry. α-Fe_2O_3 (hematite) also has a high-symmetry sixfold coordinate site with two sets of Fe-O distances (3 Fe-O at 1.95 Å and 3 Fe-O at 2.12 Å). The $3d$ feature of α-Fe_2O_3 is slightly enhanced due to a distortion from a true octahedron. Fe_3O_4 has a spiral structure with $\frac{1}{3}$ of the irons tetrahedrally coordinated and $\frac{2}{3}$ octahedrally coordinated. As expected, the $1s \rightarrow 3d$ intensity of Fe_3O_4 is enhanced due to the characteristics of the tetrahedral iron site, while the octahedral iron site gives little contribution. In the case of Fe-HRP with fivefold coordination, the intensity of the $3d$ feature is greatly enhanced over all octahedral samples. As shown in Fig. 1 and Table II, we have confirmed experimentally that the intensity of the $3d$ feature is decided to a large extent by the coordination number and to a somewhat smaller extent by the site distortion from centrosymmetry.

As shown in Fig. 2 and also indicated in Table II, the magnitudes of the $3d$ features for $YBa_2(Cu_{1-x}Fe_x)_3O_{7-\delta}$ are about 0.10 to 0.15. It is clear from the Table II that the $3d$ peaks of $YBa_2(Cu_{1-x}Fe_x)_3O_{7-\delta}$ are about an order of magnitude larger than that in model compounds with sixfold coordination and also much larger than that in Fe-HRP with fivefold coordination. The large size of these $3d$ peaks for $YBa_2(Cu_{1-x}Fe_x)_3O_{7-\delta}$ reflect the fact that the Fe site is primarily fourfold coordinated rather than fivefold coordinated. However, the intensity of the $3d$ peaks decreases smoothly with increasing Fe content. Because of its sensitivity to coordination geometry, the reduction of the magnitude of $3d$ peaks suggests that the number of Fe nearest neighbors increases with increasing Fe content.

B. Local environment of the Fe site in $YBa_2(Cu_{1-x}Fe_x)_3O_{7-\delta}$

The $\chi(k)$ data extracted from Fe K-edge EXAFS measurements of $YBa_2(Cu_{1-x}Fe_x)_3O_{7-\delta}$ are shown in Fig. 3 for three values of x ($x=0.05$, 0.10, and 0.15). The data are multiplied by k^2 to enhance the amplitude of high-k oscillations. The frequency of the sinusoidal EXAFS signal in Eq. (2) is governed by the radial distance to the backscattering atoms and the phase shift function. It can be seen in Fig. 3 that the EXAFS oscillations of these samples are similar, indicating only minor changes of the radial distances with change of Fe content. We found[22] that it is fruitful to use a phase-corrected Fourier transform (PCFT) (Ref. 12) for some systems with a mixture of different types of scatters. The advantages of using this method have been discussed elsewhere.[22] The method involves transforming the EXAFS spectrum after multiplying the data by $\exp[-\phi_i(k)]$, where the phase-shift function is empirically derived from an appropriate standard. The Fe-O PCFT k^2 weighted over a k space range from 2.3-9.0 $Å^{-1}$ are shown in Fig. 4. The empirical Fe-O phase is determined from an Fe-glycine compound.[15] Systematic changes can be seen in the magnitude of the radial structure with composition. The first peak grows with increasing Fe content. Similar changes in the second shell are also observed. The imaginary part of the PCFT's

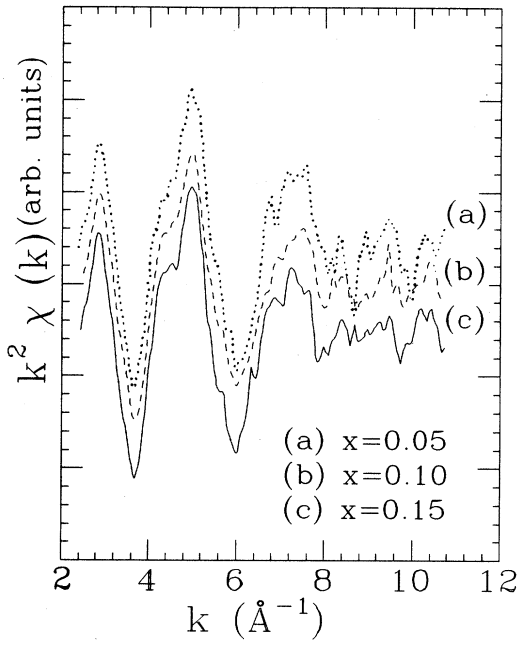

FIG. 3. $k^2\chi(k)$ for $YBa_2(Cu_{1-x}Fe_x)_3O_{7-\delta}$: (a) $x=0.05$, (dotted curve); (b) $x=0.10$, (dashed curve); and (c) $x=0.15$ (solid curve).

(data not shown here) in the first shell region (1-2.5 Å) show strong interference patterns which may result from different O coordination distances. Complicated imaginary parts in the second shell region are also seen. A quantitative analysis of the structural parameters for the first shell was performed using a nonlinear least-squares fitting technique.[12] The model compound used was the first Fe—O shell in Fe-glycine.[15] Single-, double-, and triple-distance fits were done on each sample. We found

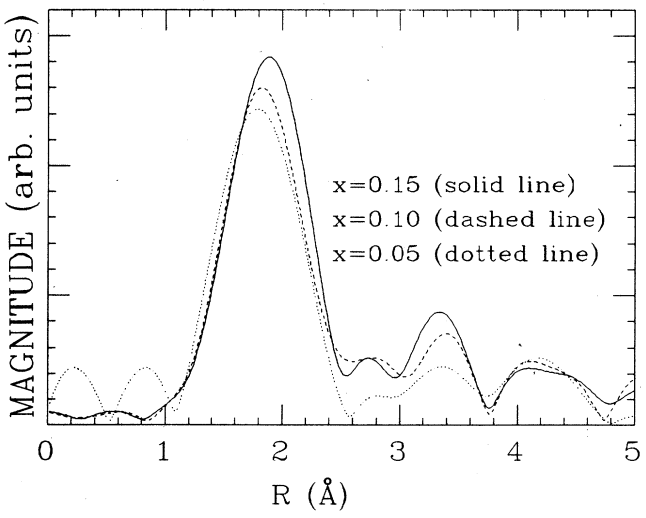

FIG. 4. The Fe-O PCFT's corresponding to Fig. 3. The k^2 transforms were taken over a k-space region of 2.3 to 9.0 $Å^{-1}$. The empirical Fe-O plane shift function was obtained from Fe glycine.[15]

that only the double-distance fit gives reasonable and consistent results. The results of the double-distance fit are listed in Table III.

In the EXAFS study of these materials, the most important issue is the assignment of the location of the Fe site. If Fe only substitutes for a Cu(2) atom at the planar site, the first shell of the Fe site should be fivefold coordinated in a square pyramidal configuration, in which there are four nearest-neighbor O atoms at a distance of about 1.94 Å along the *a*- and *b*-axis directions and a more distant O atom at a distance around 2.29 Å in the *c* direction. The second shell would contain Y, Ba, and Cu and/or Fe contributions. Based on EXAFS results indicated in Table III, this is not the case because the average total coordination number of the Fe-O pairs is close to four, but less than five. In particular, as shown in Fig. 4, the contributions of Fe-Y pairs do not occur at a corresponding distance around 3.21 Å. Therefore, our EXAFS results as well as near-edge features indicate that the contribution of the first shell is mainly due to the substitution of Fe at the Cu(1) chain site with two shorter Fe—O bonds along the *c* axis and more than two O neighbors (depending on Fe content) in the *a-b* plane. It is interesting that both Fe—O bond lengths change little with composition especially in light of the change of the lattice parameters in these samples. A major feature of this series of samples is an increase in the Fe-O in-plane coordination number. This is consistent with the changes in near-edge structure discussed previously. Based on the EXAFS results, we suggest that the number of O neighbors in the *a-b* plane increases with increasing Fe content. In fact, the decrease of the lattice parameters *c* as indicated in Table I confirm[4,6] that the oxygen content of samples increases with the rising Fe content. Therefore, we should expect that oxygen goes into empty *a*-axis sites.

There are two possibilities to explain an increased coordination number for Fe-O pairs. First, Fe only resides on the Cu(1) site with an extra oxygen distributed in the linear chain plane, which has been suggested by neutron investigators.[4,6] Second, Fe may substitute into both Cu sites for higher Fe concentrations, which has been proposed by several Mössbauer studies.[2] Our data analysis indicates that contributions from long-distance Fe-O pairs along the *c* direction in the first shell and an increase in Fe-Y pairs with increasing Fe contents in the second shell (described in the next paragraph) are absent. This rules out the latter possibility. Since the identification of the Fe site is made according to relative abundance, the amount of Fe occupying Cu(2) sites must be small and cannot be experimentally verified by this work.

Because of the absence of data for good standard compounds to provide a good transfer of phase and amplitude function and the presence of multiple scattering effects[12] involving the intervening oxygen atoms, a precise determination of the structural parameters for the second shell is difficult to achieve. In order to examine the composition effect for the second shell, an alternate approach is made by subtracting the filtered EXAFS signals for the $x=0.05$ and $x=0.10$ from the sample with $x=0.15$. In Fig. 5, the amplitude envelope of those difference EXAFS, dashed curve and dotted curve, respectively, clearly show the characteristics of the Fe-like backscattering function with some other minor contributions. This interpretation is also supported by a comparison with the Fe-Fe pairs of the second shell in FeO (solid curve). Because of backscattering amplitude effects [$F_i(k)$ in Eq. (3)], it is very easy to distinguish between a lower *z* scatterer such as Fe and heavier *Z* atoms such as Y and Ba from the shape of the EXAFS amplitudes. The difference EXAFS spectra in Fig. 5 damp out much faster at high *k* than would be expected for Y or Ba scatterers. The amplitudes also show no evidence of the resonance features[12] (amplitude minima) which occur for Y or Ba scatterers in the *k* region from 4 to 8 Å^{-1}. Thus, the different spectra do not contain any significant contributions for Y or Ba scatterers. We should point out that the current data cannot distinguish Fe backscattering from Cu at this level of accuracy. However, the second shell intensity increases with in-

TABLE III. First shell of Fe-O structural parameters.

Sample	*N*	*R* (Å)	$\Delta\sigma^2$ (Å^{-2})[a]
$x=0.05$	2.0	1.84	−0.0076
	2.2	1.94	−0.0025
$x=0.10$	2.0	1.84	−0.0067
	2.4	1.94	−0.0025
$x=0.15$	2.0	1.83	−0.0069
	2.5	1.93	−0.0019
Uncertainty	±0.2	±0.03	±0.0010

[a] Comparison with an Fe-glycine compound (Ref. 15) measured at room temperature.

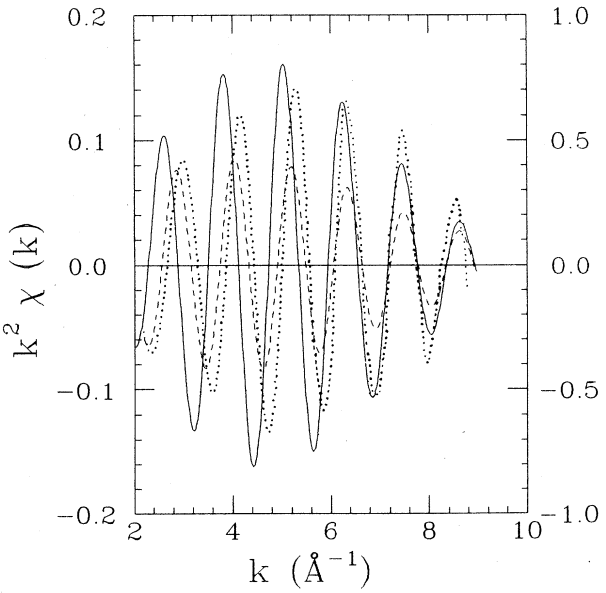

FIG. 5. Difference $k^2\chi(k)$ for second shell corresponding to Fig. 4 obtained by subtracting $x=0.05$ from $x=0.15$ data (dotted curve) and $x=0.10$ from $x=0.15$ (dashed curve). A comparison with the second shell of FeO (solid curve, label at right axis) clearly shows the characteristics of the Fe-like backscattering function for those different EXAFS spectra.

creasing Fe. This could be due to multiple scattering via extra bridging oxygens in sites along the *a* axis. The data appear to be consistent with such an explanation. If a copper atom does not want to have an extra neighboring oxygen in an *a*-axis site, the oxygen could easily be accommodated if it sits between two Fe atoms in neighboring chains. Similar Co-O-Co pairs were also found in the Co-substituted $YBa_2Cu_3O_{7-\delta}$ by Micelli *et al.*[23]

It is more important to note from the difference EXAFS that there is no evidence of an increased Fe-Y contribution with increasing Fe content which would be expected if Fe starts to reside at the Cu(2) site for higher Fe contents. Thus, this analysis supports the above argument that the substitution of Fe is mostly on the linear chain site of Cu even for higher Fe concentrations.

C. Statistical considerations of the oxygen distribution near the Fe site

It appears that the in-plane oxygen coordination of Fe increases with increasing Fe content. In principle, an individual Fe atom could have fourfold, fivefold, or sixfold (octahedral) coordination as indicated at the top of Fig. 6.

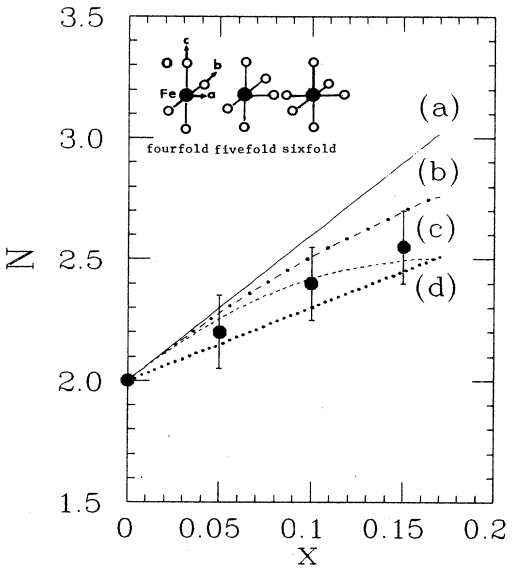

FIG. 6. Experimental values obtained from EXAFS (symbols) of the average in-plane oxygen coordination number N of Fe atoms in $YBa_2(Cu_{1-x}Fe_x)_3O_{7-\delta}$ compared with the predictions of several statistical models of oxygen distribution. (a) It is assumed that an extra oxygen is bound to every available Fe-Fe near-neighbor pair (solid curve). (b) It is assumed that an extra oxygen is bound to every available Fe-Fe near-neighbor pair, but with the constraint that no sixfold total oxygen coordination is permitted (dotted-dashed curve). (c) It is assumed that an oxygen is bound only to isolated Fe-Fe pairs and no sixfold coordination is permitted (dashed curve). (d) It is assumed that the extra-oxygen-to-iron is $\frac{1}{2}$ for all x and there is no binding of oxygen to iron (dotted curve). In all curves a–d it is assumed that Fe is substituted randomly on Cu sites in CuO planes.

It is of interest to consider the implications of the XAS results for the distributions of substitutional Fe and excess O. In particular, we will consider the distribution of the excess oxygen relative to the Fe sites.

In order to analyze properly the oxygen coordination of the substitutional Fe atoms it is necessary to know the oxygen-iron binding energy, which is not known. However, we can still draw some conclusions from the observed average in-plane oxygen coordination number N (which can take values between 2 and 4 in well-ordered $YBa_2(Cu_{1-x}Fe_x)_3O_{7-\delta}$ with total oxygen atom in excess of 7 as a function of Fe content, as shown in Fig. 6. Note that at infinite dilution ($x \rightarrow 0$), the average in-plane coordination number is 2.0. Consequently, this implies that single, isolated Fe atoms do *not* strongly bind to oxygen, for, if strong binding occurred, then N would certainly exceed 2, unless the *ratio* R of excess oxygen to Fe also vanishes as $x \rightarrow 0$. Two experimental measurements of δ using high-resolution neutron powder diffraction yield values of R of about $\frac{1}{2}$ [i.e., $R=0.56$, at $x=0.077$ (Ref. 4) and $R=0.50$ at $x=0.10$ (Ref. 6)], the value to be expected if excess O^{2-} ions compensate for the excess charge of Fe^{3+} substituted for Cu^{2+} ions. (Additional measurements of R for smaller values of x would be of great value in deciding whether or not R is $\frac{1}{2}$, independent of x, as suggested by such simple valence counting arguments. If $R \simeq \frac{1}{2}$ at infinite dilution, then the value of $N=2.0$ observed at $x=0$ implies no binding to isolated Fe atoms.

It is possible that oxygen binds to *pairs* of Fe atoms, however; note that an Fe-O-Fe unit is electrically neutral and this may be a low-energy configuration. If near-neighbor Fe-Fe pairs are required to bind an oxygen, then N can go to 2.0 as x approaches zero, even though the excess oxygen to iron ratio R remains finite. A proper analysis of this problem requires knowledge of the distribution of Fe atoms over the available Cu sites (i.e., the probability of occurrence of Fe-Fe pairs as a function of x), but we can obtain some insight by assuming a random distribution of Fe atoms, in which the probability of any given Cu site in a CuO plane being occupied by a Fe atom in $YBa_2(Cu_{1-x}Fe_x)_3O_{7-\delta}$ is $3x$. In this case, the probability of a given Fe atom (the oxygen coordination of which we are to determine) having zero, one, or two Fe near neighbors in a direction perpendicular to the CuO chain direction is $(1-3x)^2$, $6x(1-3x)$, and $9x^2$, respectively.

If it is assumed that an extra oxygen atom will always be found between any available near-neighbor pair of Fe atoms, then from the probabilities above various environments of a given Fe atoms, it is readily found that the average in-plane oxygen coordination number $N=2+6x$; this is shown in Fig. 6 as curve a and is clearly higher than the observed results. With this assumption, the ratio of extra oxygen to Fe is given by $R=6x$, which, as shown as curve a in Fig. 7, rises from zero at $x=0$ to 0.5 at $x \simeq 0.08$, in fairly good agreement with the experimental value of $\sim \frac{1}{2}$ for $x \simeq 0.077$–0.10.

The agreement of statistical models based on strong binding of the extra oxygen to Fe-Fe pairs with the experimental data for the average in-plane oxygen coordination

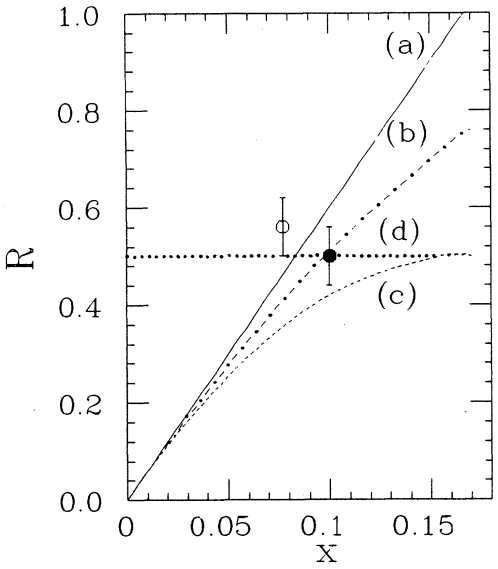

FIG. 7. Experimental values (symbols) of the extra-oxygen-to-iron ratio R obtained from high resolution neutron powder diffraction compared with the predictions of several statistical models of oxygen distribution. Filled circle is the result of Xu *et al.* (Ref. 6) and the open circle is the result of Bordet *et al.* (Ref. 4). The curves a–d are as described in the caption of Fig. 6.

N is improved if only fourfold and fivefold total oxygen coordination is permitted, but sixfold coordination is not, *i.e.*, each Fe atom can have at most one extra oxygen near neighbor. If every available near-neighbor pair of Fe atoms attracts extra oxygen, subject to the constraint of no sixfold coordination, it is found that the in-plane coordination $N=2+6x-9x^2$, shown as curve b in Fig. 6, while the extra oxygen to Fe ratio $R=6x-9x^2$, shown as curve b in Fig. 7. If only *isolated* Fe-Fe pairs (i.e., Cu-Fe-Fe-Cu but not Cu-Fe-Fe-Fe-Cu, Cu-Fe-Fe-Fe-Fe-Cu, etc.) are filled with extra oxygen, subject to the constraint of no sixfold coordination, then $N=2+6x-18x^2$, while $R=6x-18x^2$, which are shown as curves c in Figs. 6 and 7, respectively. It may be seen that in both cases curves b and c are in reasonable agreement with the experimental data for N, while the former case (all Fe-O-Fe permitted, but no sixfold coordination) is in better agreement with the data for R.

Another possibility for the oxygen distribution is that there is no binding between oxygen and iron atoms; i.e., the two populations are statistically independent and are distributed randomly. If it is also assumed that the extra oxygen which accompanies the Fe substitution is always just sufficient to compensate the extra valence of Fe^{3+}, i.e., $R=\frac{1}{2}$ for all x (shown as curve d in Fig. 7), then one obtains $N=2+3x$, shown as curve d in Fig. 6. It may be noted that this model gives fairly good agreement with the N vs x data, but perhaps not quite as good as models b and c based on strong binding to Fe-Fe pairs, while also giving good agreement with the data for R.

Thus, the conclusion which can be drawn from the x-ray absorption results of Fig. 6 is that the oxygen appears either to be bound to Fe-Fe near-neighbor pairs, or possible random distribution, but is not bound to isolated Fe atoms. Clearly more investigation of the matter is required. However, the fact that the XAS experiment is at least partially consistent with the statistical models suggests that there is a lower possibility of clustering such as Fe-O-Fe-O-Fe chains along the a axis.

IV. SUMMARY

In summary, our XAS studies of Fe substitutions for Cu in $YBa_2(Cu_{1-x}Fe_x)_3O_{7-\delta}$ lead to the following conclusions.

(1) Both the near-edge $3d$ features and the EXAFS results show that the total average coordination number of O neighbors at the Fe site is near four rather than five, indicating that Fe preferentially substitutes for Cu(1) atoms at the linear chain site. This conclusion is also supported by the fact that there is no evidence of an increased Fe-Y contribution which would be expected if some of the Fe were to occupy Cu(2) sites at higher Fe concentrations. Our observations as well as other experimental reports[1–10] indicate that the one-dimensional linear chain does not play an important role for achieving high T_c.

(2) The behavior of T_c as well as the lattice parameters varies with Fe concentration. However, the valence state of Fe (mainly 3+) and the bond lengths of the Fe-O pairs (two along the c axis and more than two in the chain plane) are insensitive to structural and compositional changes. Increasing numbers of Fe-O pairs in the chain plane are found in samples with increasing Fe content. Clearly, this is due to an attraction of more oxygen atoms distributed on the vacancies of the a axis. Furthermore, the XAS data is consistent with the hypothesis of the formation of Fe-O-Fe linkages, which is due to strong binding of the extra oxygen to Fe-Fe pairs, but not conclusive.

(3) By coupling the XAS results with statistical calculations, it is clear that the extra oxygen atoms do not form extended clusters and are possibly randomly distributed on the empty a-axis sites. Further, it is evident that the formation of sixfold coordinated (octahedral) Fe is suppressed below that of random distributions. This implication is also supported by neutron diffraction results[4–6] and some Mössbauer reports.[2] But there is no direct evidence of the necessity for the extra oxygen to be bound to Fe-Fe pairs. Hence, to gain more knowledge about the correlation between the distribution of the extra oxygen and Fe concentrations, additional study is warranted.

ACKNOWLEDGMENTS

We would like to thank Dr. James Penner-Hahn and Dr. Grant Bunker for helpful discussions and for providing their data. This research was performed under the auspices of the U.S. Department of Energy, Division of Materials Sciences, Office of Basic Energy Sciences under Contracts No. DE-AC02-76CH00016 and No. DE-AC05-80-ER10742.

*Corresponding author.

[1]Y. Maeno and T. Fujita, in *Novel Superconductivity,* edited by S. A. Wolf and V. Z. Kresin (Plenum, New York, 1987), p. 1073.

[2]Physica C **153–155** (1988), and references therein.

[3]G. Roth, G. Heger, B. Renker, J. Pannetier, V. Caignaert, M. Hervieu, and B. Raveau, Z. Phys. B **71**, 43 (1988).

[4]P. Bordet, J. L. Hodeau, P. Strobel, M. Marezio, and A. Santoro, Solid State Commun. **66**, 435 (1988).

[5]Y. K. Tao, J. S. Swinnea, A. Manthiram, J. S. Kim, J. B. Goodenough, and H. Steinfink, J. Mater. Res. **3**, 248 (1988).

[6]Youwen Xu, M. Suenaga, J. Tafto, R. L. Sabatini, A. R. Moodenbaugh, and P. Zolliker, this issue Phys. Rev. B **39**, 6667 (1989).

[7]Z. Qui, Y. W. Du, H. Tang, and J. C. Walker, J. Magn. Mater. **69**, L221 (1987).

[8]T. Tahaki, T. Komai, A. Ito, Y. Maeno, and T. Fujita, Solid State Commun. **65**, 43 (1988); E. R. Bauminger, M. Kowitt, I. Felner, and I. Nowik, *ibid.* **65**, 123 (1988); C. Saragori-Badler *et al.*, *ibid.* **66**, 381 (1988).

[9]R. Gomez *et al.*, Phys. Rev. B **36**, 7226 (1987); T. M. Tarasm *et al.*, *ibid.* **37**, 7458 (1988); E. Baggio-Savitovitch *et al.*, *ibid.* **37**, 7967 (1988); M. Eibschirtz, M. E. Lines, J. M. Tarascon, and P. Barboux, *ibid.* **38**, 2896 (1988).

[10]Youwen Xu, A. R. Moodenbaugh, R. L. Sabatini, and M. Suenaga, *Proceedings of the Symposium on High Temperature Superconductors, Reno, Nevada, 1988,* edited by D. W. Capone II, W. H. Butler, B. Batlogg, and C. W. Chu, Materials Research Symposia Series, Vol. EA-14 (Materials Research Society, Pittsburgh, 1988) p. 373.

[11]S. M. Heald, J. M. Tranquada, A. R. Moodenbaugh, and Youwen Xu, Phys. Rev. B **38**, 761 (1988); C. Y. Yang, S. M. Heald, J. M. Tranquada, A. R. Moodenbaugh, and Youwen Xu, *ibid.* **38**, 6568 (1988).

[12]*X-ray Absorption: Principles, Applications, Techniques of EXAFS, SEXAFS, and XANES,* edited by D. C. Koningsbeger and R. Prins (Wiley, New York, 1987), and references therein.

[13]C. Y. Yang, D. E. Sayers, and E. C. Theil (unpublished).

[14]J. E. Penner-Hahn *et al.*, J. Am. Chem. Soc. **108**, 7819 (1986).

[15]G. Bunker, E. A. Stern, R. E. Blankership, and W. W. Parson, J. Biol. Chem. **37**, 539 (1982).

[16]G. B. Buker, Ph. D. thesis, University of Washington, Seattle, 1984 (unpublished).

[17]V. C. Srivastara and H. L. Nigam, Coord. Chem. Rev. **9**, 275 (1972-3).

[18]G. A. Waychunas, M. J. Apted, and G. E. Brown, Jr., Phys. Chem. Miner. **10**, 1 (1983).

[19]S. M. Heald, E. A. Stern, B. Bunker, E. M. Holt, and S. L. Holt, J. Am. Chem. Soc. **101**, 67 (1979).

[20]J. E. Hahn, R. A. Scott, K. O. Hodgson, S. Doniach, S. R. Desjardin, and E. I. Solomon, Chem. Phys. Lett. **88**, 595 (1982).

[21]A. L. Roe, D. J. Schneider, R. J. Mayer, J. W. Pyrz, J. Widom, and L. Que, Jr., J. Am. Chem. Soc. **106**, 1676 (1984).

[22]C. Y. Yang, M. A. Paesler, and D. E. Sayers, Phys. Rev. B **36**, 980 (1987); *ibid.* **36**, 9160 (1987).

[23]P. F. Micelli, J. M. Tarascon, L. H. Greene, P. Barboux, F. J. Rotella, and J. D. Jorgensen, Phys. Rev. B **37**, 5932 (1988).